E-ISSN: 3050-9459
Journal of Ophthalmology and Advance Research

ATHENAEUM SCIENTIFIC PUBLISHERS

Research Article

Causal Association of ENTPD2 with Overlapping Ocular Anomalies-Membranous Cataract, Microcornea and Microphthalmia: Evidence from Whole-Exome Sequencing and *In Silico* Analysis in Two Siblings

Sankaranarayanan Rajkumar[1*], Karunakar Prashantha[3], Deepa Agrawal[1,2], Shail A Vasavada[1,2], Vaishali A Vasavada[1,2], Abhay R Vasavada[2]

[1]Department of Genetics, Iladevi Cataract and IOL Research Centre Ahmedabad 380052, Gujarat, India
[2]Department of Pediatric Ophthalmology Raghudeep Eye Hospital, Ahmedabad 380052, Gujarat, India
[3]Department of Biotechnology Dayananda Sagar College of Engineering Belagavi, Kumaraswamy Layout Bangalore, 560111 India
***Correspondence author:** Sankaranarayanan Rajkumar, MSc., Ph.D, Department of Genetics, Iladevi Cataract and IOL Research Centre Ahmedabad 380052, Gujarat, India; Email: srajkumar31@gmail.com

Citation: Rajkumar S, et al. Causal Association of ENTPD2 with Overlapping Ocular Anomalies-Membranous Cataract, Microcornea, and Microphthalmia: Evidence from Whole-Exome Sequencing and *In Silico* Analysis in Two Siblings. J Ophthalmol Adv Res. 2026;7(2):1-13.

https://doi.org/10.46889/JOAR.2026.7211

Received Date: 27-05-2026

Accepted Date: 21-06-2026

Published Date: 28-06-2026

Abstract

To investigate genetic variants associated with bilateral congenital membranous cataract, microphthalmia and microcornea in two siblings of western Indian family. Genomic DNA was extracted and subjected to Whole Exome Sequencing (WES). As none of the parents carried these phenotypes, an autosomal recessive mode of inheritance of the reported conditions was assumed. Homozygous and compound heterozygous genetic variants that were common in both siblings were screened. A functionally deleterious homozygous genetic variant (c.1319A>G; p.Tyr440Cys) in Ectonucleoside Triphosphate Diphosphohydrolase 2 (ENTPD2) gene was identified in both siblings. This variant was in apyrase conserved region 5 (ACR5) of ENTPD2, which is critical for ATP hydrolysis. Homology modeling of both wild type (Tyr440) and mutant (Cys440) ENTPD2 protein was carried out using I-TASSER and INTFold tools, respectively.

Ligand-Protein interaction studies using AutoDock Vina algorithm showed reduction in binding affinity for ATP, ADP and AMP in mutant (Cys440) ENTPD2. The Cys440 mutant likely disrupts ATP binding and hydrolysis at the ACR5 domain and might potentially influence the normal ocular development that leads to membranous cataract, microphthalmia and microcornea. Further *in-vitro* and *in-vivo* studies with the Cys440 mutant ENTPD2 are necessary to elucidate the exact disease mechanisms.

Keywords: ENTPD2; Membranous Cataract; Microcornea; Microphthalmia; Whole-Exome Sequencing; In Silico Analysis

Introduction

Congenital cataracts, characterized by varying degrees and patterns of lens opacification, are a major global cause of childhood blindness, with approximately 20,000 to 40,000 children born annually with this condition [1]. In developed countries, the prevalence is estimated to range from 1 to 6 per 10,000 live births, while higher rates have been reported in regions with increased consanguinity or environmental risk factors [2,3]. Congenital cataracts can manifest as either isolated anomalies or as part of multisystemic syndromes [4]. Genetic factors contribute significantly to

congenital cataract development, with approximately 50-90% of cases in various populations linked to inherited mutations [5,6]. In isolated congenital cataracts, mutations in genes encoding crystallins, connexins and other essential structural or developmental proteins disrupt lens transparency and fiber integrity [7]. In contrast, syndromic congenital cataracts frequently occur in association with systemic disorders such as Down syndrome, Nance-Horan syndrome, Hallermann-Streiff syndrome, Lowe syndrome and Wolframin syndrome where lens opacities result from mutations in genes responsible for broader metabolic or developmental abnormalities [8].

Approximately 12% to 18% of patients with hereditary congenital cataracts (autosomal dominant, autosomal recessive, or X-linked) also exhibit overlapping ocular conditions such as microcornea and microphthalmia [9-11]. This condition often results in significant visual impairment, necessitating early surgical intervention to prevent amblyopia and irreversible vision loss [4]. Managing these cases presents significant clinical challenges due to the complex interactions between multiple ocular abnormalities. Long-term follow-up is essential to monitor disease progression, detect emerging complications and adjust treatment strategies accordingly. Early intervention, continuous monitoring and personalized management approaches play a crucial role in preserving vision and improving long-term outcomes.

In recent years, Whole-Exome Sequencing (WES) has significantly expanded our understanding of the genetic landscape of congenital cataracts. WES have been instrumental in identifying novel candidate genes and regulatory elements involved in ocular development and homeostasis, particularly in cases presenting with overlapping conditions such as congenital cataract, microphthalmia, microcornea and coloboma [7,12].

The present study aims to investigate the genetic basis of a complex mixture of ocular conditions including membranous cataract, microphthalmia and microcornea in two siblings of Western Indian origin.

Methodology

Two siblings from western Indian family (Fig. 1), presented with tiny white spots on both the eyes (Fig. 1), were brought to Raghudeep Eye hospital. A comprehensive ophthalmic examination was performed. Visual acuity was assessed using Lea's visual acuity test and converted to the LogMAR scale. Axial Length (AL) was measured via ultrasound A-scan (immersion and contact techniques), with microphthalmia diagnosed when AL was >2 SD below the age-matched normal range. Horizontal Corneal Diameter (HCD) was measured using calipers, with microcornea defined as HCD <9.0 mm. Patients were Examined Under Anaesthesia (EUA). Type of cataract was assessed under operating microscopy. Lens with a collapsed, flattened capsule with little or no cortex or epithelium was classified as membranous cataract [13]. Posterior segment evaluation was done to identify Persistent Fetal Vasculature (PFV) Ultrasound B-scan was performed when fundus visibility was obstructed. Ocular assessments included Anterior Chamber (AC) depth, IOP, gonioscopy, engorged iris vessels, synechiae, retinal detachment and vitreous hemorrhage. Demographic and etiological data were recorded.

The study was approved by the Institutional Ethics Committee (ICIRC/IEC/2012-2015) and adhered to the Declaration of Helsinki guidelines. A written informed consent was obtained from the parents and the siblings were monitored or followed up for nearly two decades.

Sibling 1 (Fig. 1), a 7-month-old female, was born full-term without complications. Initial ophthalmic evaluation revealed bilateral microcornea (8.5 mm corneal diameter on both meridian), microphthalmia (axial length: 14.6 mm OD, 16.1 mm OS), shallow anterior chambers (2.3 mm OD, 1.7 mm OS) and constant esotropia (20-25°). She was diagnosed with bilateral membranous cataract (Fig. 1) with dense anterior capsular plaques (Fig. 1). Pars plana lensectomy and vitrectomy were performed without Intraocular Lens (IOL) implantation.

Postoperative complications included corneal haziness, posterior capsular opacification, posterior synechiae and an abnormal iris pattern. Fundus examination revealed Optic Disc pallor (OD) and an increased cup-to-disc ratio (0.8 OD). By age 20, she had progressive visual decline (CF 2.5 m OD, 0.5 m OS) and secondary glaucoma, requiring anti-glaucoma treatment since 2010. Fundus evaluations of the left eye remained limited due to persistent pupillary constriction.

Sibling 2 (Fig. 1), an 8-month-old male, was born full-term without complications. Initial evaluation revealed bilateral microcornea (8.5 mm), shallow anterior chambers (2.5mm bilateral), constant esotropia (35°) and horizontal nystagmus. Axial lengths were 18.6 mm (OD) and 17.4 mm (OS). Visual acuity could not be assessed due to absence of light fixation. He was diagnosed with bilateral membranous cataract (Fig. 1) with dense anterior capsular plaques (Fig. 1). Pars plana lensectomy and vitrectomy were performed without Intraocular Lens (IOL) implantation. Postoperative complications included corneal decompensation, persistent esotropia, posterior capsular opacification and synechiae in the OS. In subsequent follow-ups mesodermal dysgenesis (partly absence of iris), angle closure and pinhole pupils were identified. He had congenital elevated IOP, necessitating trabeculotomy (OS) and ongoing Timolol treatment.

Fundus examinations were often limited due to pupillary constriction, though cup-to-disc ratios remained normal (0.2-0.3). Now 19 years old, he has experienced progressive visual decline, with final recorded acuity of 0.75 LogMAR (OD) and CF at 0.5 m (OS). Anterior lens capsules with plaques were surgically obtained, washed in phosphate-buffered saline (PBS, pH 7.4) and spread on chilled glass slides. Capsules were fixed in Carnoy's fixative (3:1 methanol-acetic acid), stained with Hematoxylin and Eosin (H&E) and observed under microscopic (Axioskope 2, Carl Zeiss, Germany). Images were captured for analysis of plaque morphology, distribution and epithelial cell arrangement.

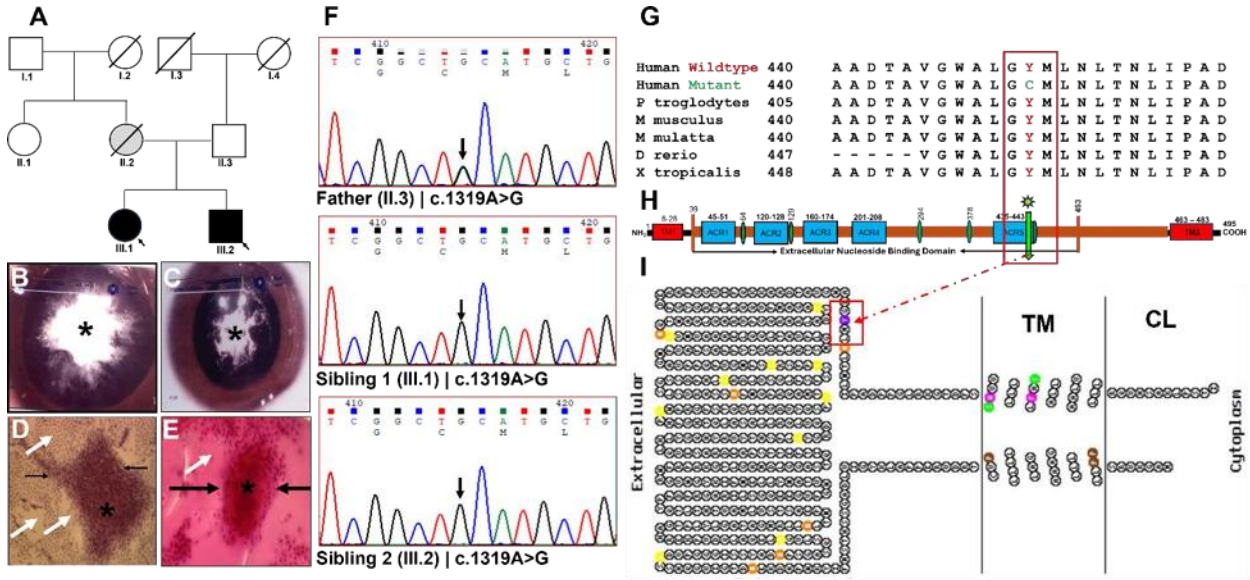

Figure 1: (A) The three generation family pedigree shows two affected siblings (III.1 and III.2) with non-consanguineous parents (II.2 and II.3). The mother (II.2) had a history of cataract (light shade), is deceased, and no further clinical details are available. The father (II.3) has bilateral visual impairment due to trauma, though detailed clinical information is unavailable. Sibling 1 (III.1) & Sibling 2(III.2) presented with bilateral congenital membranous cataract (B& C, respectively) and dense anterior capsular plaque (D & E, respectively).D&E: Hematoxylin and Eosin (H&E) staining of the anterior lens capsule revealed a thick plaque formed by aggregated differentiated and undifferentiated lens epithelial cells(*), creating a dense fibrous mass. Scattered epithelial cells across the capsule led to significant gaps (white arrows), indicating disrupted cell-cell coordination and communication. These findings suggest abnormal cell proliferation and impaired adhesion, contributing to the pathological changes in the lens. (F) Sanger sequencing chromatogram illustrates the nucleotide change (c.1319A>G) in ENTPD2 gene; Father (II.3) harbors heterozygous genotype, while both the siblings harbor homozygous alternate genotype. (G) The nucleotide variant c.1319A>G resulted in change in amino acid from tyrosine to cysteine at position 440 (p.Tyr440Cys). Sequence homology mapping by Clustal W showed that the amino acid tyrosine is conserved across different species in the hierarchy. (H) Cartoon illustrates theregions and numbers of amino acids in different domains; cytoplasmic: 1- 7, transmembrane-1: 8-28, extracellular: 29-462, transmembrane-2: 463-483, cytoplasmic: 484- 495, and five major apyrase conserved region (ACR1-5) of ectonucleoside triphosphate diphosphohydrolase 2 protein. The variant tyrosine to cysteine at position 440 is located in the ACR5 shown by arrow and Asterick mark. (I) Transmembrane protein display of ENTPD2. The mutated amino acid is highlighted with purple color (red box). TM: Transmembrane domain, CL: cytoplasmic loop. Amino acid residues in Orange: N-glycosylation sites, Yellow: cysteine residues, Green: OH residues, Magenta: aromatic residues, Brown: Proline residues.

Whole Exome Sequencing (WES)

Peripheral blood (2 mL) was collected via venipuncture and genomic DNA (gDNA) was isolated using the salt extraction method [14]. A total of 300 ng of gDNA was fragmented using a Covaris M220 Focused Ultrasonicator (150-200 bp fragments), end-repaired and dA-tailed. Indexing adapters were ligated and purification was performed using AmpureXP beads. The adapter-ligated DNA was PCR-amplified using AmpliTaqGold PCR Mastermix (95°C for 10 min, 6 cycles of 95°C for 30 sec, 65°C for 30 sec, 72°C for 30 sec, final extension at 72°C for 5 min).Target enrichment was conducted using SureSelect V5+UTR exome capture probes (Agilent Technologies, USA), followed by post-hybridization PCR and purification with AmpureXP beads. The enriched library was analyzed using the 4200 TapeStation System (Agilent Technologies) for size distribution and quality assessment. Paired-end sequencing (150 bp read length) was performed on an Illumina NextSeq500 platform at Scigenome (Kochi, India), achieving a mean depth of ~100X, ensuring high-quality data for downstream analysis.

Data Processing and Selection of Variants

Bioinformatics analysis of WES data was performed using an in-house pipeline. Raw sequencing data in FASTQ format were assessed for quality using FastQC v0.11.5. Reads were aligned to the human reference genome GRCh37p13 using Burrows-Wheeler Aligner (BWA)-MEM v0.7.17with default parameters and alignment quality was assessed using SAM tools v1.9.

Duplicate reads were removed using Picard v2.2.1 and variant calling was performed using the Genome Analysis Toolkit (GATK) HaplotypeCaller. Variant Call Files (VCFs) were annotated using Franklin tool and variants were classified as pathogenic, likely pathogenic, uncertain significance, or benign based on the American College of Medical Genetics and Genomics (ACMG) guidelines.

Variants were filtered based on a quality Phred score ≥30, Quality by Depth (QD) ≥2X and depth of coverage (DP) ≥20X. Variants retained for further analysis included non-synonymous variants, frameshift variants, those introducing stop codon gains or losses and splice-site variants (donor +2, acceptor -8). Further selection was based on and Minor Allele Frequency (MAF) ≤0.01, aggregated across 1000 Genomes, ExAC and gnomAD and an aggregated prediction score ≥0.5 and a CADD score ≥20.0. Variants predicted to significantly disrupt protein function were validated using Sanger sequencing.

Homology Modeling of Wild Type and Mutant ENTPD2

Sequence homology and conservation analyses of Ectonucleoside Triphosphate Diphosphohydrolase 2 (ENTPD2) across various species were conducted using Clustal W. Notably, a 3D protein model of human ENTPD2 has not been established experimentally and is absent from public Protein Data Bank (PDB). Therefore, the primary amino acid sequence of human ENTPD2 (Q9Y5L3) was retrieved from the UniProt Database in FASTA format and the mutant sequence was generated by substituting tyrosine with cysteine at position 440. We predicted the secondary and tertiary structures of both wild-type (Tyr440) and mutant (Cys440) using the improved ModFOLD7 algorithm of IntFold5 and I-TASSER web servers [15-18]. The C-score of the predicted models was utilized to select the best candidate for further refinement. Final model refinement and energy minimization were executed using the ModRefiner tool, which employs a two-step process: first, minimizing the energy of the backbone, followed by the addition of side chains and subsequent energy minimization of both the side chains and backbone [19]. The validation of the structural integrity of the modeled proteins was conducted using RAMPAGE, a Ramachandran Plot Generator Server.

Prediction of Binding Efficiency of ATP, ADP and AMP with Wild Type and Mutant ENTPD2

We docked three ligands-ATP, ADP and AMP-using AutoDock Vina [20]. For the wild type ENTPD2, the grid box was centered at coordinates (25.574, 31.810, 20.132) with dimensions 30.84 × 22.32 × 22.32. For the mutant ENTPD2, the grid box was centered at (85.683, 84.945, 88.794) with dimensions 25.32 × 23.56 × 31.56. Docking simulations were run with an exhaustive setting of 8. All nine generated conformations were analyzed for hydrogen bonding and other interactions using LIGPLOT+ software [21]. The resulting complexes were visualized using PyMOL.

Results

Analysis of Anterior Capsular Plaques

Hematoxylin and Eosin (H&E) staining of the anterior lens capsule (Fig. 1) revealed a dense fibrous plaque characterised by aggregation of both differentiated and undifferentiated lens epithelial cells (marked by asterick). A disrupted cell-cell

coordination and communication was observed by the presence of scattered epithelial cells and gaps (white arrows) across the lens capsule. These findings suggest abnormal cell proliferation and impaired adhesion, contributing to the pathological changes in the lens.

Identification of Genetic Variants

Whole exome sequencing identified 51 genetic variants, including 46 exonic and 5 splice-site (acceptor 3 and donor 2) across 50 genes shared by both siblings (Table 1). As the diagnosed phenotypes were absent in the parents, a recessive mode of inheritance was assumed and we prioritized homozygous and compound heterozygous variants common to both. Among them, TEX9 exhibited compound heterozygosity for splice site variants (c.27+1G>C, c.396-2A>G), while ENTPD2 had a homozygous variant (c.1319A>G) in coding region.

TEX9gene was excluded from the candidature as no known ocular diseases were associated with this gene. While ENTPD2, was selected as a potential candidate as it was shown to have linked with microphthalmia. Sanger sequencing confirmed homozygosity in both siblings (Fig.1, middle and bottom panels) and heterozygosity in their father (Fig.1, top panel), suggesting a possible autosomal recessive mode of inheritance. The c.1319A>G (rs549794840) variant is rare, with a Minor Allele Frequency (MAF) of 0.002 globally and <0.05 in South Asians. Only four homozygous cases (three females and one male) were reported in gnomAD.

This c.1319A>G variant results in a Tyr440Cys substitution in ENTPD2, affecting a highly conserved (Fig. 1) apyrase conserved region 5 (ACR5) (Fig. 1) responsible for ATP hydrolysis in the extracellular domain (Fig. 1). *In silico* predictions, including CADD (26.8), SIFT (0.0), PolyPhen2 (1.0) and PROVEAN (-8.25), classified it as deleterious, suggesting a potential impact on protein activity. MutPred2 revealed a loss of α-helix (prediction score of 0.61, p=0.39) in ENTPD2.

Homology Modeling and Functional Impact Prediction of ENTPD2 on Substrate Binding To identify the best-fitting protein model for subsequent protein-ligand docking analysis, Ramachandran plots were generated for both the wild-type and mutant structural models developed using I-TASSER and IntFold. The optimal model was selected based on the percentage of residues in the favourable region (expected cutoff ~98%), allowable region (cutoff ~2%) and outlier region (<2%), as shown in the Ramachandran plots.

For the wild-type (Tyr440) model, IntFold displayed 97.2% of residues (472 amino acids) in the favourable region, 2.4% (12 amino acids) in the allowable region and 0.4% (2 amino acids) in the outlier region. In contrast, I-TASSER generated a model with 91.9% (453 amino acids) in the favourable region, 5.9% (29 amino acids) in the allowable region and 2.2% (11 amino acids) in the outlier region (Fig. 2).

For the mutant (Cys440) model, I-TASSER produced a structure with 94.3% (465 amino acids) in the favourable region, 4.3% (21 amino acids) in the allowable region and 1.4% (7 amino acids) in the outlier region, whereas IntFold yielded a model with 91.9% (453 amino acids) in the favourable region, 6.3% (31 amino acids) in the allowable region and 1.8% (9 amino acids) in the outlier region (Fig. 2). Therefore, the IntFold-derived wild-type (Tyr440) model and the I- TASSER-derived mutant (Cys440) model were selected for further docking analysis (Supplementary Table S1).

Superimposition of the wild-type and mutant homology models revealed a Root-Mean-Square Deviation (RMSD) of 1.37 Å for the local region (amino acids 31-289) and 13.3 Å for the global region (amino acids 2-495) (http://superpose.wishartlab.com/) (Fig. 2). Additionally, the distance between the binding domain and the substrate was significantly different, measuring 10.3 Å for the wild-type (Tyr440) (Fig. 2) and 7.4 Å for the mutant (Cys440) (Fig. 2), indicating a notable structural alteration in the mutant protein.

Interaction of ATP, ADP and AMP with Wild-Type and Mutant ENTPD2

An in-silico ligand-binding analysis using AutoDock Vina showed a lower (more negative) binding energy score for ATP (-8.3 kcal/mol), ADP (-8.5 kcal/mol) and AMP (-8.6 kcal/mol) in the wild-type (Tyr440) ENTPD2 (Fig. 3). In contrast, the mutant (Cys440) ENTPD2 exhibited a higher (less negative) binding energy, indicating weaker substrate binding: ATP (-7.6 kcal/mol) (Fig. 3), ADP (-7.5 kcal/mol) (Fig. 3) and AMP (-7.1 kcal/mol) (Fig. 3). These findings suggest that ATP, ADP and AMP exhibit a stronger affinity for the wild type (Tyr440) compared to the mutant (Cys440). Additionally, the minimum binding distance was

greater in the wild-type (ATP: 8.9 Å, ADP: 9.5 Å, AMP: 9.3 Å) (Fig. 3) compared to the mutant (ATP: 8.3 Å, ADP: 8.6 Å, AMP: 8.2 Å) (Fig. 3). These structural differences further highlight the impaired binding efficiency of the mutant ENTPD2 (Supplementary Table S2).

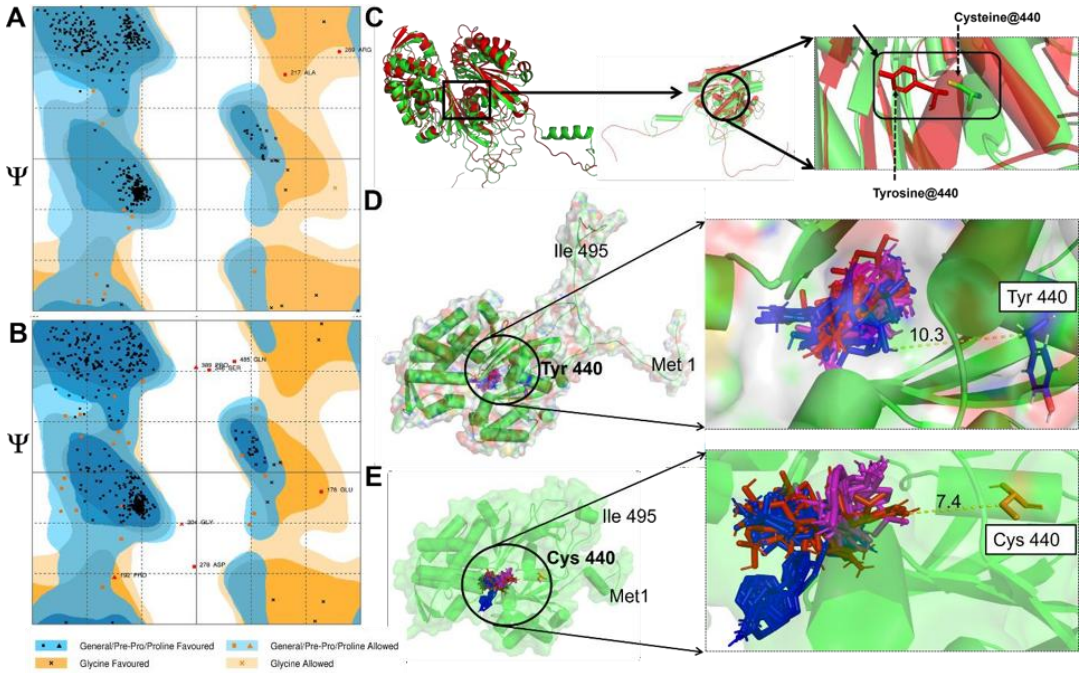

Figure 2: Ramachandran Plots of the modeled ENTPD2 protein;(A) wildtype and (B) mutant obtained from RAMPAGE. Models for both wild type (Tyr440) and mutant (Cys440) amino acids were generated using IntFold and I-TASSER in silico tools. The best fitting model for both wild type and mutant was selected based on the number of residues in favored region (expected cutoff value ~98%), number of residues in allowed region (cutoff ~2%), and number of residues in outlier region (<2%) as shown in Ramachandran plots. C) Superposition of wild-type and mutant ENTPD2 (left panel). Molecular docking interaction of ligands with D) wildtype Tyr440 and E) Mutant Cys 440 residues of ENTPD2 protein. The distance (A°) between the ligands and the amino acids is shown by dotted lines. Ligands ATP (red), ADP (blue) and AMP (magenta).

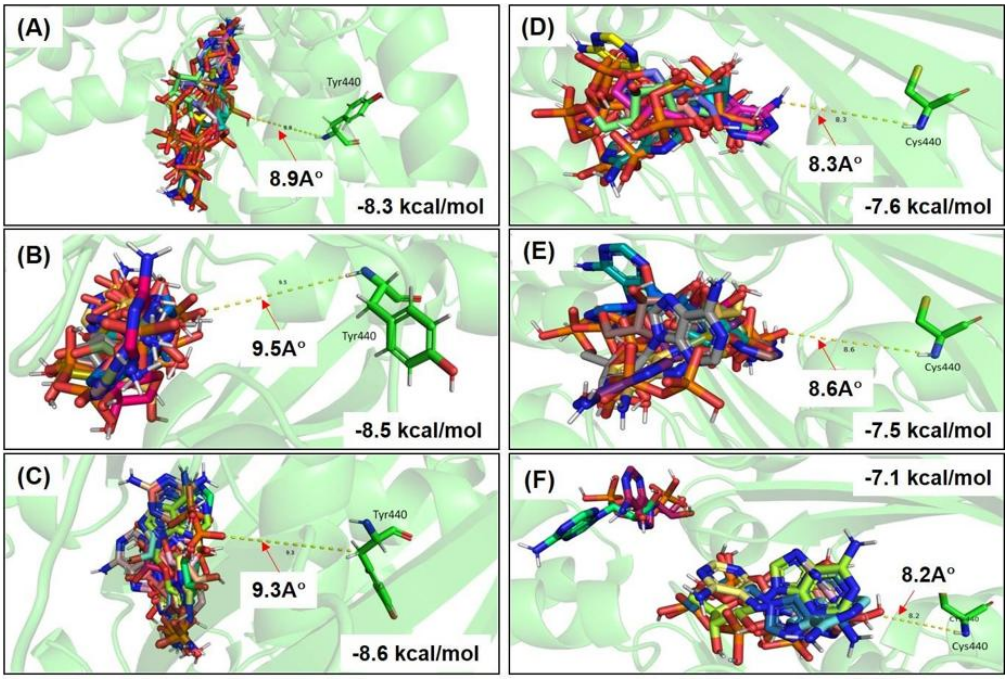

Figure 3: Molecular docking interaction of ligands ATP (A & D), ADP (B & E) and AMP (C & F) with wildtype Tyr440 (A-C) and mutant Cys 440 (D-F) of ENTPD2 protein. The minimum distance (A◎) and binding energy (kcal/mol) between the ligands

ATP (red), ADP (blue) and AMP (magenta) and the amino acids are shown by dotted lines and red arrow. The inlet boxes represent the distance (A°) and binding energy (kcal/mol) between ligand and amino acid.

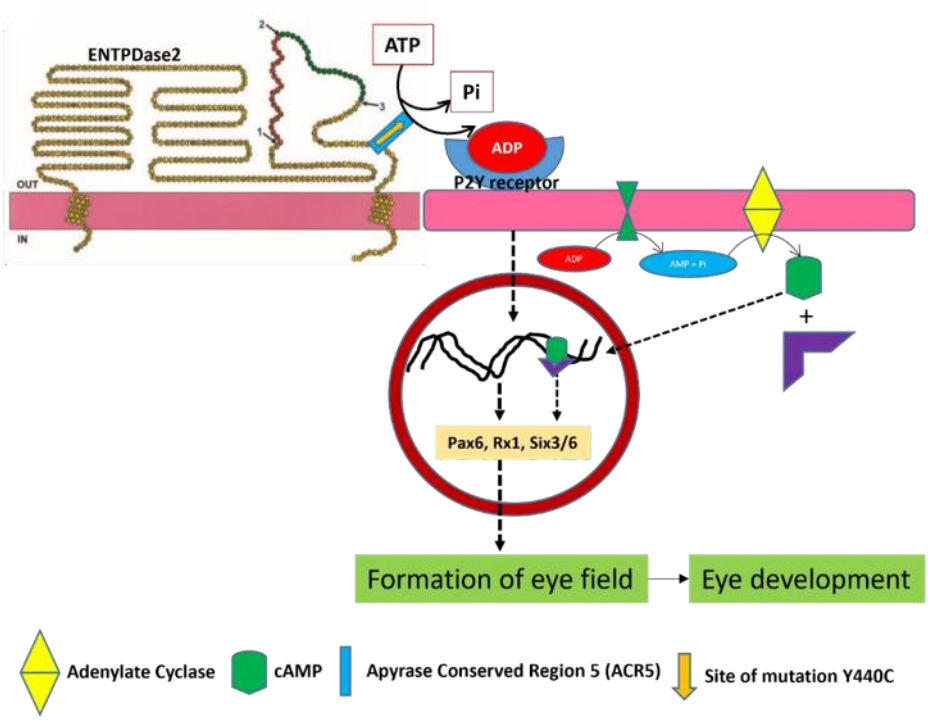

Figure 4: Hypothetical model of ENTPD2's mechanism in regulating gene expression and initiating eye field formation and development. ENTPD2, an ectoenzyme that hydrolyzes extracellular ATP to ADP, plays a crucial role in purinergic signaling pathways that regulate cellular proliferation and differentiation during early eye development. These processes are essential for forming ocular structures, including the retina, lens, and cornea, through molecular factors like Pax6, Rx1, and Six3. The identified Y440C mutation in ENTPD2 may cause steric hindrance at the Apyrase Conserved Region 5 (ACR5), leading to impaired ATP binding and a disruption in the purinergic signaling cascade. This dysfunction could interfere with key pathways that regulate gene expression, affecting the development of neural crest cells and other progenitor cells involved in ocular formation. As a result, the mutation may contribute to the overlapping ocular phenotypes observed in the siblings, such as membranous cataracts, microphthalmia and microcornea. The model further suggests that ENTPD2 may act upstream of eye field transcription factors, including PAX6, which is critical for lens placode formation. Although no mutations in PAX6 were detected in the siblings, ENTPD2's role in regulating PAX6 expression could explain the observed phenotypes. This highlights the potential significance of ENTPD2 in ocular development, although conflicting evidence regarding its role underscores the need for further investigation into its precise contributions to eye pathology.

Gene	Chr#	Transcript Ref	Nucleotide	AA Change	Zygosity	dbSNP_ID	MAF	APS
ABCD4	14	NM_005050.4	c.1042C>T	p.Arg348Trp	Het	rs147795328	0.00	0.50
ABCG5	2	NM_022436.3	c.1259T>G	p.Val420Gly	Het	rs773630787	0.00	0.68
AHCYL1	1	NM_006621.7	c.1142C>T	p.Thr381Ile	Het	rs201916372	0.00	0.62
ARHGEF38	4	NM_001242729.2	c.1772G>A	p.Arg591His	Het	rs939877535	0.00	0.56
CBR1	21	NM_001757.4	c.23C>G	p.Ala8Gly	Het	rs566688474	-	0.84
CCN4	8	NM_003882.4	c.413C>T	p.Pro138Leu	Het	rs564097534	0.00	0.69
CDH23	10	NM_022124.6	c.4672G>A	p.Gly1558Arg	Het	rs760432842	0.00	0.85
ENTPD2	9	NM_203468.3	c.1319A>G	p.Tyr440Cys	Hom	rs549794840	0.00	0.59
FGFR1	8	NM_023110.3	c.66G>C	p.Arg22Ser	Het	rs17175750	0.00	0.55
GABPB1	15	NM_001320910.2	c.619+1G>T	-	Het	rs80042819	0.00	0.80
GABRP	5	NM_014211.3	c.830T>C	p.Ile277Thr	Het	-	-	0.87

GANC	15	NM_198141.2	c.2306T>A	p.Ile769Asn	Het	rs79004308	0.01	0.87
GAS6	13	NM_000820.4	c.1382C>T	p.Thr461Met	Het	rs202234400	0.00	0.52
GJA3	13	NM_021954.4	c.92T>A	p.Ile31Asn	Het	-	-	0.87
HBP1	7	NM_012257.4	c.910G>A	p.Val304Ile	Het	rs1266469544	0.00	0.70
HECTD3	1	NM_024602.6	c.976G>A	p.Val326Met	Het	rs370539478	0.00	0.53
INSR	19	NM_000208.4	c.3034G>A	p.Val1012Met	Het	rs1799816	0.01	0.69
ITGA6	2	NM_001316306.2	c.418G>A	p.Gly140Ser	Het	rs74728869	0.01	0.79
KCNAB3	17	NM_004732.4	c.353A>G	p.Tyr118Cys	Het	rs527702902	0.00	0.60
KRT13	17	NM_153490.3	c.1028C>T	p.Ala343Val	Het	rs199762312	0.00	0.50
KRT27	17	NM_181537.4	c.847-1G>A	-	Het	rs187944199	0.01	0.80
LAMA1	18	NM_005559.4	c.8839G>T	p.Gly2947Cys	Het	rs140080119	0.00	0.87
LEF1	4	NM_016269.5	c.844G>A	p.Val282Met	Het	rs151041212	0.00	0.51
LHX3	9	NM_178138.6	c.265A>C	p.Lys89Gln	Het	-	-	0.86
LRP1B	2	NM_018557.3	c.8527C>G	p.Arg2843Gly	Het	rs529890891	0.00	0.62
MLYCD	16	NM_012213.3	c.193G>A	p.Glu65Lys	Het	rs755172155	0.00	0.73
MSRA	8	NM_012331.5	c.424G>C	p.Asp142His	Het	rs371090925	0.00	0.63
MUC6	11	NM_005961.3	c.1249G>A	p.Gly417Ser	Het	rs533027075	0.00	0.66
NAE1	16	NM_003905.4	c.611T>C	p.Met204Thr	Het	rs555207416	0.00	0.64
NET1	10	NM_001047160.3	c.1283G>A	p.Arg428Gln	Het	rs780188577	0.00	0.56
NGB	14	NM_021257.4	c.175C>T	p.Pro59Ser	Het	rs558334380	0.00	0.70
NRCAM	7	NM_001037132.4	c.2648T>C	p.Ile883Thr	Het	-	-	0.70
PMVK	1	NM_006556.4	c.388C>T	p.Arg130Cys	Het	rs150445298	0.00	0.64
PPFIA2	12	NM_003625.5	c.3344G>A	p.Arg1115His	Het	rs61756413	0.01	0.61
PPIF	10	NM_005729.4	c.286C>T	p.His96Tyr	Het	rs747106167	0.00	0.68
PRF1	10	NM_001083116.3	c.632C>T	p.Ala211Val	Het	rs368524364	0.00	0.65
PTCH1	9	NM_000264.5	c.2485G>A	p.Val829Met	Het	rs201125580	0.00	0.67
RECQL	12	NM_002907.4	c.833C>G	p.Thr278Arg	Het	rs372732456	0.00	0.54
RECQL5	17	NM_004259.7	c.2828G>A	p.Arg943His	Het	rs200535477	0.00	0.70
ROR2	9	NM_004560.4	c.1712A>G	p.His571Arg	Het	rs376970201	0.00	0.56
RYR3	15	NM_001036.6	c.6617A>C	p.Asn2206Thr	Het	rs181264765	0.00	0.86
SELENON	1	NM_020451.3	c.1162A>G	p.Ser388Gly	Het	rs562843129	0.00	0.53
SEMA3A	7	NM_006080.3	c.506G>T	p.Ser169Ile	Het	rs746633015	0.00	0.50
SLC12A4	16	NM_005072.5	c.1726A>G	p.Met576Val	Het	rs749137904	0.00	0.59
SLC1A7	1	NM_006671.6	c.1362-2A>G	-	Het	-	-	0.80
SPATA48	7	NM_001161834.3	c.1086dup	p.Ala363Cysfs*22	Het	rs767486080	0.00	0.80
STAB2	12	NM_017564.10	c.3140A>T	p.Lys1047Ile	Het	rs569064317	0.00	0.72
TAF1C	16	NM_001243156.2	c.1169C>T	p.Pro390Leu	Het	rs757052865	0.00	0.54
TEX9	15	NM_198524.3	c.27+1G>C	-	Het	rs747435082	0.00	0.80
TEX9	15	NM_198524.3	c.396-2A>G	-	Het	rs553964995	0.00	0.80
TXNRD2	22	NM_006440.5	c.1499G>T	p.Cys500Phe	Het	rs554063995	0.00	0.84
AA Change: Amino acid change, MAF refers to the Aggregated Minor Allele Frequency across 1000 Genomes (1000g), ExAC,								

gnomAD- exome, and gnomAD-genome. APS: aggregated functional prediction score (higher the score indicates higher impact on protein function).APS (Aggregated Functional Prediction Score) is derived from REVEL and MetaLR scores. The APS ranges from 0 to 1 and is classified as very strong benign (<0.003), strong benign (0.003-0.016), moderate benign (0.016-0.183), supporting benign (0.183-0.290), uncertain (0.290-0.644), supporting pathogenic (0.644-0.773), moderate pathogenic (0.773-0.932), and strong pathogenic (>0.932).

Table 1: List of genetic variants found common in both siblings.

Discussion

The two siblings reported here were diagnosed with overlapping ocular phenotypes, including membranous cataract, microphthalmia and microcornea. Membranous cataract is a rare and severe form of congenital cataract characterized by a collapsed, flattened capsule with little or no cortex or epithelium on the lens [13]. Additional clinical features included dense anterior lens capsular plaques, nystagmus, strabismus (esotropia), shallow anterior chamber, elevated Intraocular Pressure (IOP), miotic pupils, abnormal iris patterns and early-onset progressive vision loss. Notably, the younger sibling exhibited primary congenital glaucoma. These conditions were absent in their parents and other family members.

In a previous study on the same siblings, based on Sanger Sequencing, we reported a novel heterozygous missense variant (c.92T>A; p.Ile31Asn) in the GJA3 gene [22]. Gap Junction, alpha 3 (GJA3), known as connexin 46, is responsible for the formation of gap junction (hemichannels)in the lens and its mutations are solely associated with cataracts. We believe that the genetic variant in GJA3 is likely to be associated with the disrupted cell-cell coordination and communication as seen in the anterior capsular plaques (Fig. 1) and might partly be associated with cataract in both siblings and their mother. However, given the broader spectrum of phenotypes observed in these siblings, we believe that GJA3 genetic variant alone may not be accounted for the same. Therefore, in the present study, we employed whole-exome sequencing to investigate additional genetic variants potentially contributing to or associated with these distinct ocular phenotypes. Given the similarity in their overlapping features and the absence of these conditions in their parents, we anticipated an autosomal recessive inheritance pattern and prioritized genes harbouring homozygous or compound heterozygous variants. Following stringent quality control and variant screening procedures, we identified a homozygous missense variant in the ENTPD2 gene.

ENTPD2, also known as NTPDase2, is located on chromosome 9q34.3 and contains nine exons. It encodes ecto-nucleoside triphosphate diphosphohydrolase 2, a type II transmembrane protein with a single transmembrane domain, a short cytoplasmic N-terminus and a large extracellular catalytic domain containing five conserved apyrase domains (Fig. 1). ENTPD2 regulates extracellular nucleotide levels by hydrolysing nucleoside triphosphates (ATP, UTP) into their diphosphate forms (ADP, UDP) via its apyrase conserved regions (ACR1-5), a key process in purinergic signalling through P1 and P2 receptors. Purines such as ATP and purinergic signalling pathways play significant roles in the physiology and pathology of diverse ocular structures, including the cornea (epithelial, neuronal processes, stromal keratinocytes), choroid, retina (RPE, retinal neurons, astrocytes, Müller cells), optic nerve head (nerve sheath), lens, trabecular meshwork and lacrimal gland [23-29]. The role of ENTPD2 in regulating purinergic signalling pathways in these structures has also been demonstrated [28,30-33].

The c.1319A>G variant in ENTPD2 resulted in the substitution of tyrosine with cysteine at position 440 (p.Tyr440Cys). In silico protein modelling indicated that this substitution within the fifth Apyrase Conserved Region (ACR5) altered molecular configuration, affecting structural stability (Fig. 2) and functional capacity (Fig. 3). Molecular docking studies with ATP, ADP and AMP revealed a significant reduction in binding efficiency with the mutant ENTPD2 protein. Mateo, et al., demonstrated through *in-vitro* transfection and enzymatic analysis that ENTPD2 variants Cys399 to Ser399 and Asn443 to Asp443 led to a complete loss or reduction of ectonucleotidase activity [34]. Similarly, the variant observed in this study, Tyr440 to Cys440 mutation in ENTPD2 could significantly impair the binding of ATP, ADP and AMP due to loss of π-stacking, H-bonding capacity and introduction of a chemically reactive thiol group.

Biochemical and physiological factors such as redox state, pH and local microenvironment can further exacerbate binding inefficiency by promoting thiol modification or structural distortion. Previous studies have associated duplications at chromosome 9q34, where ENTPD2gene resides, with various eye defects, including microphthalmia, deep-set eyes and exotropia (35). Masse, et al., demonstrated in a Xenopus laevis model that overexpression of ENTPD2 led to the formation of ectopic eye-like structures by upregulating critical transcription factors, including Pax6, Rx1 and Six3. Conversely, downregulation of ENTPD2 reduced Pax6 and Rx1 expression, resulting in a small eye phenotype, suggesting that ENTPD2 acts upstream of key

transcription factors involved in eye field development [36]. PAX6, a downstream target of ENTPD2, is essential for lens placode formation, a critical step in lens development. PAX6 mutations have been linked to several ocular disorders, including autosomal dominant aniridia (OMIM:106210), anterior segment dysgenesis 5 (OMIM:604229) and microphthalmia/coloboma 12 (OMIM:120200). The phenotypic spectrum associated with PAX6 mutations closely aligns with the overlapping ocular conditions observed in our study subjects. Although no PAX6 variants were detected in the siblings, we attribute the observed phenotypes to the ENTPD2genetic variant, given its known role in regulating PAX6 expression. A hypothetical model illustrating the regulation of key eye development genes is presented (Fig. 4). Despite conflicting evidence from a single study, which questioned ENTPD2's role in eye development, numerous studies support its involvement in ocular function [37]. The well-established role of purinergic signalling pathways in ocular physiology and the demonstrated presence and role of ENTPD2 in activating these pathways further support its potential role in ocular disease development [23-33]. Functional impact predictions from in silico analysis in this study suggest a reduced interaction between mutant ENTPD2 (Cys440) and its substrates (ATP, ADP and AMP), implicating ENTPD2 in ocular diseases.

A wide array of genes has been implicated in the overlapping phenotypes of congenital cataract, microcornea and microphthalmia. Mutations in crystallin genes such as CRYAA, CRYAB, CRYBB1, CRYBB2, CRYGC, CRYGD and CRYBA4, genes involved in lens cell communication and water transport, such as GJA3, GJA8 and MIP, transcription factors like PAX6, PITX3, FOXE3, SOX2, OTX2, VSX2 and RAX, genes influences lens differentiation and structural integrity such as HSF4, EPHA2, BFSP2,and CHMP4B, genes regulating axial length and eye size such as MFRP, PRSS56,and TMEM98 and genes associated with more severe or syndromic forms of ocular dysgenesis such as NDP, BEST1, FOXG1, GLI2,and COL4A1/COL4A2 have been reported in congenital cataracts in association with microcornea or microphthalmia [7,9-12,38]. Interestingly, we did not find any genetic variants in these reported candidate genes, except GJA3 in these two siblings. Therefore, we attribute the ENTPD2 gene and its variant to the phenotypes presented in the siblings.

In summary, the Cys440mutant in ENTPD2 likely reduces ecto-nucleotidase activity in the developing ocular environment, potentially disrupting purinergic signalling pathways essential for the development of the eye globe, cornea and lens. These findings suggest that ENTPD2 is a promising candidate gene for the overlapping ocular conditions observed in the siblings, particularly membranous cataract, microphthalmia and microcornea. Further research is required to elucidate how ENTPD2genetic variants affect these molecular processes and their precise role in the pathogenesis of these ocular conditions.

Conclusion

This study is the first of its kind highlighting the potential role of the ENTPD2 gene and its variant in bilateral membranous cataract, microcornea and microphthalmia. It underscores two critical aspects of patient management: (1) congenital cataracts may indicate underlying complications, necessitating long-term follow-up for paediatric patients diagnosed with congenital cataracts and (2) incorporating genetic testing, such as whole-exome sequencing, into clinical practice is essential for understanding the genetic mechanisms underlying complex or overlapping phenotypes.

Conflict of Interest

The authors declared no potential conflicts of interest with respect to the research, authorship and/or publication of this article.

Funding Statement

The study was supported by grants from the Indian Council of Medical Research, New Delhi, India (file nos. 5/4/6/10/Oph. 11-NCD II and 5/4/6/2012-RMC).

Acknowledgement

The authors have no acknowledgments to declare.

Data Availability Statement

The data supporting the findings of this study are available from the corresponding author upon reasonable request.

Ethical Statement

The project did not meet the definition of human subject research under the preview of the IRB according to federal regulations and therefore was exempt.

Informed Consent Statement

Informed consent was obtained from all participants included in the study.

Authors' Contributions

Conception and design: Sankaranarayanan Rajkumar, Abhay R Vasavada, Deepa Agarwal
Analysis and interpretation of the data: Sankaranarayanan Rajkumar, Deepa Agarwal, Shail A Vasavada, Karunakar Prashantha
Drafting of the paper: Sankaranarayanan Rajkumar, Karunakar Prashantha, Vaishali A Vasavada
Revising it critically for intellectual content: Sankaranarayanan Rajkumar, Abhay R Vasavada, Vaishali A Vasavada
Final approval of the version to be published: All authors agree to be accountable for all aspects of the work.

References

1. Bell SJ, Oluonye N, Harding P, Moosajee M. Congenital cataract: a guide to genetic and clinical management. Ther Adv Rare Dis. 2020;1:2633004020938061.
2. Rahi JS, Dezateux C. National cross sectional study of detection of congenital and infantile cataract in the United Kingdom: role of childhood screening and surveillance. BMJ. 1999;318(7180):362-5.
3. Sheeladevi S, Lawrenson JG, Fielder AR, Suttle CM. Global prevalence of childhood cataract: a systematic review. Eye (Lond). 2016;30(9):1160-9.
4. Lambert SR, Drack AV. Infantile cataracts. Surv Ophthalmol. 1996;40(6):427-58.
5. Hejtmancik JF. Congenital cataracts and their molecular genetics. Semin Cell Dev Biol. 2008;19(2):134-49.
6. Shiels A, Hejtmancik JF. Molecular genetics of cataract. Prog Mol Biol Transl Sci. 2015;134:203-18.
7. Gillespie RL, O'Sullivan J, Ashworth J, Bhaskar S, Williams S, Biswas S, et al. Personalized diagnosis and management of congenital cataract by next-generation sequencing. Ophthalmology. 2014;121(11):2124-37.
8. Francis PJ, Berry V, Bhattacharya SS, Moore AT. The genetics of childhood cataract. J Med Genet. 2000;37(7):481-8.
9. Abouzeid H, Meire FM, Osman I, ElShakankiri N, Bolay S, Munier FL, et al. A new locus for congenital cataract, microcornea, microphthalmia and atypical iris coloboma maps to chromosome 2. Ophthalmology. 2009;116(1):154-62.
10. Hansen L, Yao W, Eiberg H, Kjaer KW, Baggesen K, Hejtmancik JF, et al. Genetic heterogeneity in microcornea-cataract: five novel mutations in CRYAA, CRYGD and GJA8. Invest Ophthalmol Vis Sci. 2007;48(9):3937-44.
11. Bardakjian TM, Schneider A. The genetics of anophthalmia and microphthalmia. Curr Opin Ophthalmol. 2011;22(5):309-313.
12. Reis LM, Semina EV. Genetic landscape of isolated pediatric cataracts: extreme heterogeneity and variable inheritance patterns within genes. Hum Genet. 2019;138(8-9):847-63.
13. Duke-Elder S. Normal and abnormal development. Part 2: congenital deformities. In: System of Ophthalmology. St Louis: CV Mosby. 1963;(3):752-6.
14. Rajkumar S, Vasavada AR, Praveen MR, Ananthan R, Reddy GB, Tripathi H, et al. Exploration of molecular factors impairing superoxide dismutase isoforms activity in human senile cataractous lenses. Invest Ophthalmol Vis Sci. 2013;54(9):6224-33.
15. McGuffin LJ, Adiyaman R, Maghrabi AHA, Shuid AN, Brackenridge DA, Nealon JO, et al. IntFOLD: an integrated web resource for high performance protein structure and function prediction. Nucleic Acids Res. 2019;47(W1):W408-13.
16. Roy A, Kucukural A, Zhang Y. I-TASSER: a unified platform for automated protein structure and function prediction. Nat Protoc. 2010;5(4):725-38.
17. Yang J, Yan R, Roy A, Xu D, Poisson J, Zhang Y. The I-TASSER suite: protein structure and function prediction. Nat Methods. 2015;12(1):7-8.
18. Yang J, Zhang Y. I-TASSER server: new development for protein structure and function predictions. Nucleic Acids Res. 2015;43(W1):W174-81.
19. Xu D, Zhang Y. Improving the physical realism and structural accuracy of protein models by a two-step atomic-level energy minimization. Biophys J. 2011;101(10):2525-34.
20. Trott O, Olson AJ. AutoDock Vina: improving the speed and accuracy of docking with a new scoring function, efficient optimization and multithreading. J Comput Chem. 2010;31(2):455-61.

21. Laskowski RA, Swindells MB. LigPlot+: multiple ligand-protein interaction diagrams for drug discovery. J Chem Inf Model. 2011;51(10):2778-86.
22. Vidya NG, Rajkumar S, Vasavada AR. Genetic investigation of ocular developmental genes in 52 patients with anophthalmia/microphthalmia. Ophthalmic Genet. 2018;39(3):344-52.
23. Peral A, Gallar J, Pintor J. Adenine nucleotide effect on intraocular pressure: involvement of the parasympathetic nervous system. Exp Eye Res. 2009;89(1):63-70.
24. Li A, Leung CT, Peterson-Yantorno K, Stamer WD, Civan MM. Cytoskeletal dependence of adenosine triphosphate release by human trabecular meshwork cells. Invest Ophthalmol Vis Sci. 2011;52(11):7996-8005.
25. Wurm A, Pannicke T, Iandiev I, Francke M, Hollborn M, Wiedemann P, et al. Purinergic signaling involved in Müller cell function in the mammalian retina. Prog Retin Eye Res. 2011;30(5):324-42.
26. Guzman-Aranguez A, Santano C, Martin-Gil A, Fonseca B, Pintor J. Nucleotides in the eye: focus on functional aspects and therapeutic perspectives. J Pharmacol Exp Ther. 2013;345(3):331-41.
27. Sanderson J, Dartt DA, Trinkaus-Randall V, Pintor J, Civan MM, Delamere NA, et al. Purines in the eye: recent evidence for the physiological and pathological role of purines in the RPE, retinal neurons, astrocytes, Müller cells, lens, trabecular meshwork, cornea and lacrimal gland. Exp Eye Res. 2014;127:270-9.
28. Lu W, Hu H, Sévigny J, Gabelt BT, Kaufman PL, Johnson EC, et al. Rat, mouse and primate models of chronic glaucoma show sustained elevation of extracellular ATP and altered purinergic signaling in the posterior eye. Invest Ophthalmol Vis Sci. 2015;56(5):3075-83.
29. Santiago AR, Madeira MH, Boia R, Aires ID, Rodrigues-Neves AC, Santos PF, et al. Keep an eye on adenosine: its role in retinal inflammation. Pharmacol Ther. 2020;210:107513.
30. Reigada D, Lu W, Zhang X, Friedman C, Pendrak K, McGlinn A, et al. Degradation of extracellular ATP by the retinal pigment epithelium. Am J Physiol Cell Physiol. 2005;289(3):C617-24.
31. Mitchell CH, Reigada D. Purinergic signalling in the subretinal space: a role in the communication between the retina and the RPE. Purinergic Signal. 2008;4(2):101-7.
32. Ricatti MJ, Alfie LD, Lavoie EG, Sévigny J, Schwarzbaum PJ, Faillace MP. Immunocytochemical localization of NTPDases1 and 2 in the neural retina of mouse and zebrafish. Synapse. 2009;63(4):291-307.
33. Losenkova K, Takeda A, Ragauskas S, Cerrada-Gimenez M, Vähätupa M, Kaja S, et al. CD73 controls ocular adenosine levels and protects retina from light-induced phototoxicity. Cell Mol Life Sci. 2022;79(3):152.
34. Mateo J, Kreda S, Henry CE, Harden TK, Boyer JL. Requirement of Cys399 for processing of the human ecto-ATPase (NTPDase2) and its implications for determination of the activities of splice variants of the enzyme. J Biol Chem. 2003;278(41):39960-8.
35. Allderdice PW, Eales B, Onyett H, Sprague W, Henderson K, Lefeuvre PA, et al. Duplication 9q34 syndrome. Am J Hum Genet. 1983;35(5):1005-19.
36. Massé K, Bhamra S, Eason R, Dale N, Jones EA. Purine-mediated signalling triggers eye development. Nature. 2007;449(7165):1058-62.
37. Gampe K, Haverkamp S, Robson SC, Gachet C, Hüser L, Acker-Palmer A, et al. NTPDase2 and the P2Y1 receptor are not required for mammalian eye formation. Purinergic Signal. 2015;11(1):155-60.
38. Shiels A. Through the Cat-Map Gateway: a brief history of cataract genetics. Genes (Basel). 2024;15(6):785.

Supplementary Files

Rampage Results- Modrefiner	Wildtype ENTPD2 (Tyr440)		Mutant ENTPD2 (Cys440)	
	I-TASSER	IntFold	I-TASSER	IntFold
Number of residues in favored region (~98% expected)	453 (91.9%)	479 (97.2%)	465 (94.3%)	453 (91.9%)
Number of residues in allowed region (~2% expected)	29 (5.9%)	12 (2.4%)	21 (4.3%)	31 (6.3%)
Number of residues in outlier region	11 (2.2%)	2 (0.4%)	7 (1.4%)	9 (1.8%)

Supplementary Table S1: Cuttoff parameters from RAMPAGE (Ramachandran Plots) used for the selection of wildtype and mutant models for ENTPD2.

Ligands	Wildtype ENTPD2(Tyr440)		Mutant ENTPD2(Cys440)	
	Binding Energy (kcal/mol)	Minimum Distance (Å)	Binding Energy (kcal/mol)	Minimum Distance (Å)
ATP	-8.3	8.9	-7.6	8.3
ADP	-8.5	9.5	-7.5	8.6
AMP	-8.6	9.3	-7.1	8.2

Supplementary Table S2: Binding affinity and the minimum distance between the docked conformation of ligands with Wildtype and mutant ENTPD2.